Biochemical and Biophysical Research Communications 424 (2012) 439–445

Contents lists available at SciVerse ScienceDirect

Biochemical and Biophysical Research Communications

journal homepage: www.elsevier.com/locate/ybbrc

L-type calcium channels play a crucial role in the proliferation and osteogenic differentiation of bone marrow mesenchymal stem cells

Li Wen [a,1], Yu Wang [b,1], Huan Wang [a,1], Lingmin Kong [c], Liang Zhang [a], Xin Chen [d], Yin Ding [a,*]

[a] Department of Orthodontics, School of Stomatology, Fourth Military Medical University, Xi'an 710032, China
[b] Department of Oncology, Xijing Hospital, Fourth Military Medical University, Xi'an 710032, China
[c] Department of Fundamental Medicine, Cell Engineering Research Centre, Fourth Military Medical University, Xi'an 710032, China
[d] Department of General Dentistry, The 174th Hospital of Chinese PLA, Xiamen 361003, China

ARTICLE INFO

Article history:
Received 18 June 2012
Available online 3 July 2012

Keywords:
L-type Ca^{2+} channel
Mesenchymal stem cells
Cell proliferation
Osteogenic differentiation

ABSTRACT

L-type voltage-dependent Ca^{2+} channels ($VDCC_L$) play an important role in the maintenance of intracellular calcium homeostasis, and influence multiple cellular processes. They have been confirmed to contribute to the functional activities of osteoblasts. Recently, $VDCC_L$ expression was reported in mesenchymal stem cells (MSCs), but the role of $VDCC_L$ in MSCs is still undetermined. The aim of this study was to determine whether $VDCC_L$ may be regarded as a new regulator in the proliferation and osteogenic differentiation of rat MSC (rMSCs). In this study, we examined functional Ca^{2+} currents (I_{Ca}) and mRNA expression of $VDCC_L$ in rMSCs, and then suppressed $VDCC_L$ using nifedipine (Nif), a $VDCC_L$ blocker, to investigate its role in rMSCs. The proliferation and osteogenic differentiation of MSCs were analyzed by MTT, flow cytometry, alkaline phosphatase (ALP), Alizarin Red S staining, RT-PCR, and real-time PCR assays. We found that Nif exerts antiproliferative and apoptosis-inducing effects on rMSCs. ALP activity and mineralized nodules were significantly decreased after Nif treatment. Moreover, the mRNA levels of the osteogenic markers, osteocalcin (OCN), bone sialoprotein (BSP), and runt-related transcription factor 2 (Runx2), were also down-regulated. In addition, we transfected α1C-siRNA into the cells to further confirm the role of $VDCC_L$ in rMSCs, and a similar effect on osteogenesis was found. These results suggest that $VDCC_L$ plays a crucial role in the proliferation and osteogenic differentiation of rMSCs.

1. Introduction

Mesenchymal stem cells (MSCs) are multipotent stem cells that can self-renew and differentiate into various cell types, such as osteoblasts, chondrocytes, adipocytes, and endothelial cells, depending on their parental tissue type and subsequent culture conditions [1,2]. However, the mechanism of MSC proliferation and osteogenic differentiation *in vitro* is not well understood. During proliferation and differentiation of osteoblasts, many processes are modulated by a variety of hormones, cytokines, genes, or chemicals [3]. Among these processes, calcium ions (Ca^{2+}) play a critical role in regulating cellular functions [4]. Ca^{2+} influx into cells can generate biological signals, which can modulate crucial intracellular processes, such as hormone secretion, synaptic transmission, and gene regulation.

L-type voltage-dependent Ca^{2+} channels ($VDCC_L$) are important factors for Ca^{2+} influx in many exci cells [5] as well as several types of non-excitable cells [6,7]. It has been demonstrated that there are functional Nif-sensitive $VDCC_L$ in rat osteoblasts [8] and in a small population of rat MSCs [9]. $VDCC_L$ are large transmembrane multiprotein complexes that couple membrane depolarization to cellular calcium entry. These channels are composed of α1, α2, δ, β subunits, and in some cases a γ subunit [10]. The α1 subunit of the VDCC1 family is the target of organic Ca^{2+} channel blockers and the site of Ca^{2+} influx, and possess the pharmacological characteristics and functional properties of the Ca^{2+} channel for voltage sensing, ion permeability, and drug binding [11]. In addition, the extracellular α2 subunit facilitates the assembly of α1 at the cell surface and modulates channel kinetics [12].

Investigating whether $VDCC_L$ affects the ability of proliferation and osteogenic differentiation of MSCs is important for elucidating the mechanism responsible for maintaining cellular functional activities. In this study, we assessed the gene expression and functional I_{Ca} of $VDCC_L$ in rat MSCs, and investigated the effects of $VDCC_L$ on cellular proliferation and osteogenic differentiation of rMSCs *in vitro*.

2. Materials and methods

2.1. Isolation and culture

MSCs were isolated from aspirates of bone marrow harvested from the femur and tibia of one-month-old Sprague Dawley rats. The cells were isolated by density gradient centrifugation, and then

* Corresponding author. Fax: +86 29 8322 3047.
E-mail address: dingyin@fmmu.edu.cn (Y. Ding).
[1] These authors contributed equally to this work.

0006-291X/$ - see front matter © 2012 Elsevier Inc. All rights reserved.
http://dx.doi.org/10.1016/j.bbrc.2012.06.128

seeded into 75 cm^2 flasks containing a-MEM (Gibco, Rockville, MD) supplemented with 2 mM GlutaMAX, 10 U/ml penicillin, 100 μg/ml streptomycin (all from Sigma–Aldrich, St. Louis, MO, USA), and 10% fetal bovine serum (FBS; Gibco). The cultures were maintained at 37 °C in a humidified 5% CO_2 incubator. The culture medium was changed after 48 h to remove non-adherent cells, and then changed every 3 days thereafter. When cells reached 80–90% confluency, they were passaged by Trypsin-EDTA solution (0.25% trypsin, 1 mM EDTA; Sigma). Cells in the third passage were used for subsequent experiments.

2.2. Electrical recording

The $VDCC_L$ currents were recorded using the whole-cell patch-clamp technique [13]. In brief, cells were constantly perfused with bath solution containing 120 mM tetraethylammonium chloride, 10 mM CsCl, 10 mM HEPES, 2 mM $CaCl_2$, 1 mM $MgCl_2$, and 10 mM Glucose (pH 7.2, CsOH). Ba^{2+} currents were measured in a solution containing 10 mM Ba^{2+} instead of 2 mM Ca^{2+}. To validate the $VDCC_L$ current and examine the effects of $VDCC_L$ blockers on the channel, the bath solution was supplemented with 0.01, 0.1, or 1 μM Nif (Sigma). The inward sodium current (I_{Na}) was eliminated by substituting tetraethylammonium chloride (TEA-Cl) for NaCl. The basic pipette solution for the I_{Ca} study contained 90 mM Cs-methanesulfonate, 20 mM CsCl, 10 mM HEPES, 4 mM Mg-ATP, 0.4 mM Tris-GTP, 10 mM EGTA, and 3 mM $CaCl_2$ (pH 7.2, CsOH). Patch pipettes achieving a resistance of 1–3 MΩ when filled with the pipette solution were used. All experiments were conducted at room temperature (21–23 °C). The signals were recorded and stored in a Clampfit utility program (pCLAMP 10.0, Molecular Devices, LLC, Sunnyvale, CA, USA).

2.3. MTT assay for cell proliferation

The cells were seeded into 96-well plates at a density of 5×10^3 cells/well in 200 μl medium. After 24 h in culture, the medium was replaced with fresh medium with or without Nif. The MTT assay was performed every 24 h. Briefly, 20 μl MTT (5 mg/ml) solution was added to each well, and the plates were incubated at 37 °C and 5% CO_2 for an additional 4 h. The medium was then removed and 150 μl/well DMSO was added to dissolve the formazan by pipetting up and down several times. An enzyme-linked immunosorbent assay was used to measure the values of optical densities (OD) at a wavelength of 490 nm.

2.4. Flow cytometry for cell cycle and apoptosis analyses

rMSCs were cultured in medium supplemented with or without the Nif, channel blocker, in 25 cm^2 flasks. After 3 days, rMSCs in the two groups were detached and centrifuged. For the cell cycle assay, cells were washed with ice-cold PBS and then centrifuged for 5 min at 1000*g*. The cells were then fixed with 2 ml ice-cold 70% alcohol and 1 ml ice-cold PBS, and incubated at 4 °C for a minimum of 30 min. For cell apoptosis analysis, the Annexin V-FITC Apoptosis Detection Kit (Oncogene, San Diego, CA) was used. The cells were rinsed with ice-cold PBS, resuspended in 500 μl of binding buffer, and then incubated for 30 min at 4 °C with 5 μl of Annexin V and 2 μl of PI solution. All samples were analyzed by flow cytometry (FACSCalibur, Becton Dickinson).

2.5. Induction of osteogenic differentiation

The cells were plated in 12-well plates at a density of 5×10^4 cells/well. After cells reached 70% confluence, the medium was replaced with osteogenic medium (ODM, 10% FBS/α-MEM, 10 nM dexamethasone, 10 mM β-glycerophosphate, and 50 μM ascorbic acid, Sigma), with or without Nif, respectively. The medium was changed every 3 days.

2.6. Alizarin Red S staining and quantification

Alizarin Red S staining was used to analyze calcium phosphate formation after 21 days of osteogenic differentiation. After removing the ODM, the cells were gently washed with PBS and fixed in 10% formalin solution for 15 min at room temperature. The cells were washed with distilled water and incubated in Alizarin Red S (Sigma) for 20–30 min in the dark. They were then washed twice with PBS to remove excess dye. Image-Pro Plus 5.0 was used to analyze the quantity of nodule areas.

2.7. ALP assay and staining

The cells were seeded at a density of 5×10^4 cells/well in 12-well plates and then treated with ODM or ODM supplemented with Nif. After 10 days in culture, ALP staining was performed using the BCIP/NBT Alkaline Phosphatase Color Development Kit (Beyotime, Haimen, China). An ALP activity assay kit (Beyotime, Haimen, China) was used to analyze ALP enzymatic activity. The cells were seeded in 96-well plates at a density of 5×10^3 cells/well. ALP activity was analyzed on culture days 1, 3, 5, and 7, according to the manufacturer's instructions. The results were measured at 520 nm using an enzyme-linked immunosorbent assay.

2.8. RT-PCR and real-time PCR

Total RNA was extracted from cultured cells using the TriZol reagent (Invitrogen, Carlsbad, CA) according to the manufacturer's directions. Complementary DNA (cDNA) synthesis was obtained by using SuperScript II reverse transcriptase (Invitrogen). PCR was performed on α1C and α2 of $VDCC_L$, as well as glyceraldehyde 3-phosphate dehydrogenase (GAPDH) templates using an ExTaq polymerase kit (Takara, Shuzo, Japan). The thermal cycling conditions were 5 min at 95 °C, followed by 35 cycles at 55 °C for 20 s, 57 °C for 20 s, and 60 °C for 40 s. After amplification, the PCR products were resolved on a 1.5% agarose gel and visualized under UV illumination (BioRad) after staining with ethidium bromide. Real-time PCR was carried out with an ABI 7500 real-time PCR system (Applied Biosystems) using SYBR Premix Ex Tag™ (TaKaRa). The PCR amplification for OCN, BSP, Runx2, and GAPDH was performed with the following cycling conditions: denaturation at 95 °C for 2 min, followed by 45 cycles at 95 °C for 10 s and 60 °C for 40 s. Quantification of gene expression was analyzed using the comparative threshold cycle (ΔΔCt) method [14], and relative expression levels were quantified by normalizing to GAPDH expression. The primer sets used in RT-PCR and real-time PCR are listed in Table 1.

2.9. RNA interference

The small interfering RNA (siRNA) duplexes targeting the rat α1C gene of $VDCC_L$ were purchased from GenePharma (Huntingdon, UK) with siRNA entrez gene ID 199812 (sense, 5′-CCAUUUUCACCAUUGAAAU-3′ and antisense, 5′-AUUUCAAUGGUGAAAAUGG-3′). The AllStars Negative Control siRNA (1027281, Qiagen, Hilden, Germany) was used as a negative control. For gene transfection, rMSCs were grown in 6-well plates at a density of 1×10^6 cells/ml for 24 h, and then the cells were transfected with 30 nM siRNA using HiPerFect transfection reagent for siRNA (Qiagen). The medium was changed after 24 h and the cells were assayed for gene knockdown 48 h post-transfection. The cells were also cultured in ODM 24, 48, and 72 h post-transfection, and total RNA was extracted for gene expression analysis.

Table 1
Primers sequences and expected size of PCR products.

Genes	Forward primer	Reverse primer	Size (bp)
α1C	5′-CGAGCCCAGAAAAGAAACAG-3′	5′-ACTGCCTTTTCCTTAAGGTGCA-3′	271
α2	5′-CTCTGAGATGTTAGAAACCCTT-3′	5′-CTTCTCCTCCATCCGTGA-3′	272
OCN	5′-AGGACCCTCTCTCTGCTCAC-3′	5′-AACGGTGGTGCCATAGATGC-3′	294
BSP	5′-GCGAATTCTGAACGGGTTTCAGCAGAC-3′	5′-GCGAATTCTGGTGGTAGTAATAATCCT-3′	272
Runx2	5′-GCCGGGAATGATGAGAACTA-3′	5′-GAGGCAGAAGTCAGAGGTGG-3′	582
GAPDH	5′-GTGCTGAGTATGTCGTGGAG-3′	5′-GTCTTCTGAGTGGCAGTGAT-3′	289

2.10. Statistics

The results were expressed as mean ± standard deviation. Significance of differences between the two groups was tested by the independent samples *t*-test. Differences among three or more groups were analyzed by one-way analysis of variance (ANOVA) followed by a Bonferroni post hoc test. A $P < 0.05$ was considered statistically significant.

3. Results

3.1. Basal characterization of rMSCs

Elongated spindle-shaped or rhomboid rMSCs grew colonially and displayed a rather homogeneous confluent population (Fig. 1A). The cells were immunopositive (>81.5%) for CD90 and CD105, but were negative (<2%) for CD34 and CD45 (Fig. 1D). Moreover, the cells differentiated into adipocytes and osteoblasts when cultured in induction media (Fig. 1B and C).

3.2. Molecular expression and current recordings of $VDCC_L$ in rMSCs

RT-PCR was used to measure the mRNA expression of the α1C and α2 subunits of $VDCC_L$ in rMSCs (Fig. 2A). The I_{Ca} in rMSCs measured by patch-clamp and electrophysiological recordings showed that the I_{Ca} was produced by depolarization from a holding potential of −70 mV, and were activated at a membrane potential −40 mV, which peaked at +10 mV and substantially increased when Ca^{2+} was substituted for Ba^{2+} (10 mM; I_{Ba}) (Fig. 2B and C). After Nif was added to the bath solution, the I_{Ca} was completely blocked, partially blocked, or barely blocked by 1, 0.1, and 0.01 μM Nif, respectively (Fig. 2D).

3.3. Effects of $VDCC_L$ on cell proliferation

We examined the effect of Nif on the viability of rMSCs using an MTT assay. Nif displayed dose- and time-dependent inhibition on the growth of rMSCs (Fig. 3A). The cell cycle of rMSCs was detected by flow cytometry (Fig. 3C and D). We found that Nif treatment substantially decreased the cellular DNA content of rMSCs treated with 1 μM Nif (Fig. 3B), while cells treated with 0.1 μM Nif showed a slight but non-significant decrease (date not shown). Together, these results suggest that inhibition of $VDCC_L$ can down-regulate rMSCs proliferation. We subsequently assessed whether the inhibited proliferative effect of Nif was related to apoptosis. The flow cytometry results showed that Nif greatly enhanced the apoptosis of rMSCs in a dose-dependent manner (Fig. 3E and F).

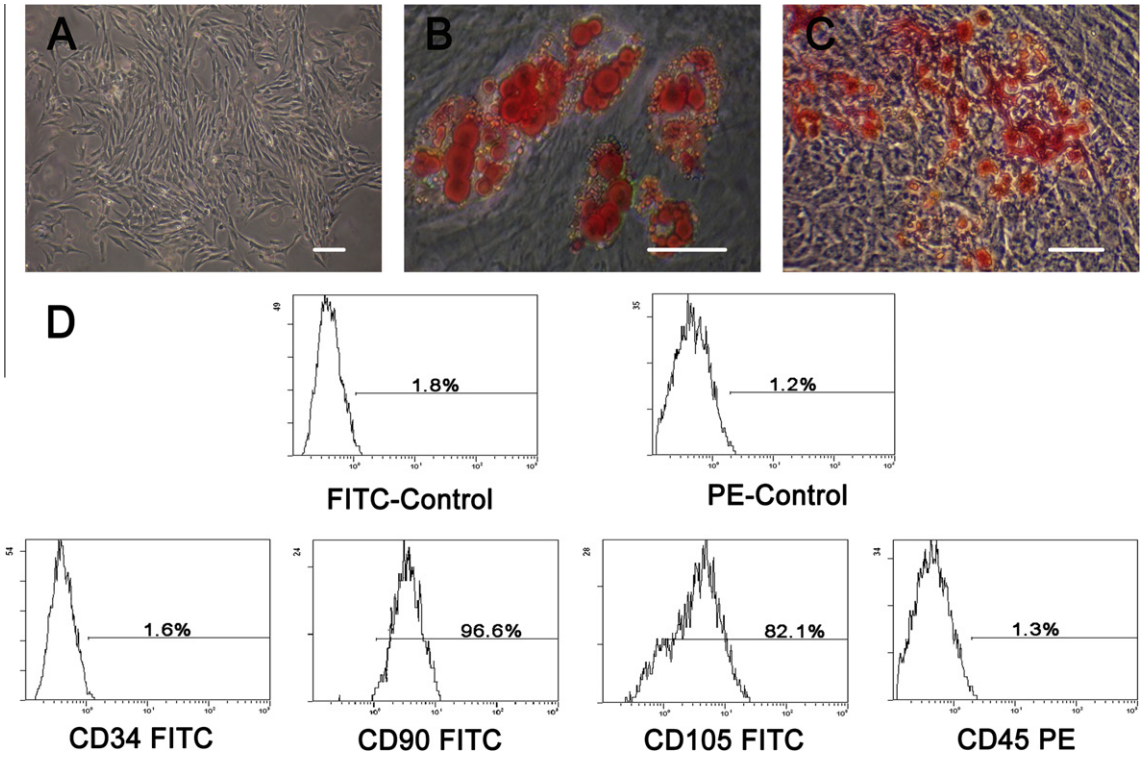

Fig. 1. (A) Morphology of rMSCs after culturing the cells for 5 days. (B) Adipogenic induction for 10 days. The cells were stained with oil Red O solution and show a lipid laden adipocyte phenotype. (C) Osteogenic induction for 21 days. Mineralized nodules were detected after Alizarin Red S staining. Bars = 20 μm. (D) The expression of stem cell surface markers assessed by flow cytometry. (For interpretation of the references to colour in this figure legend, the reader is referred to the web version of this article.)

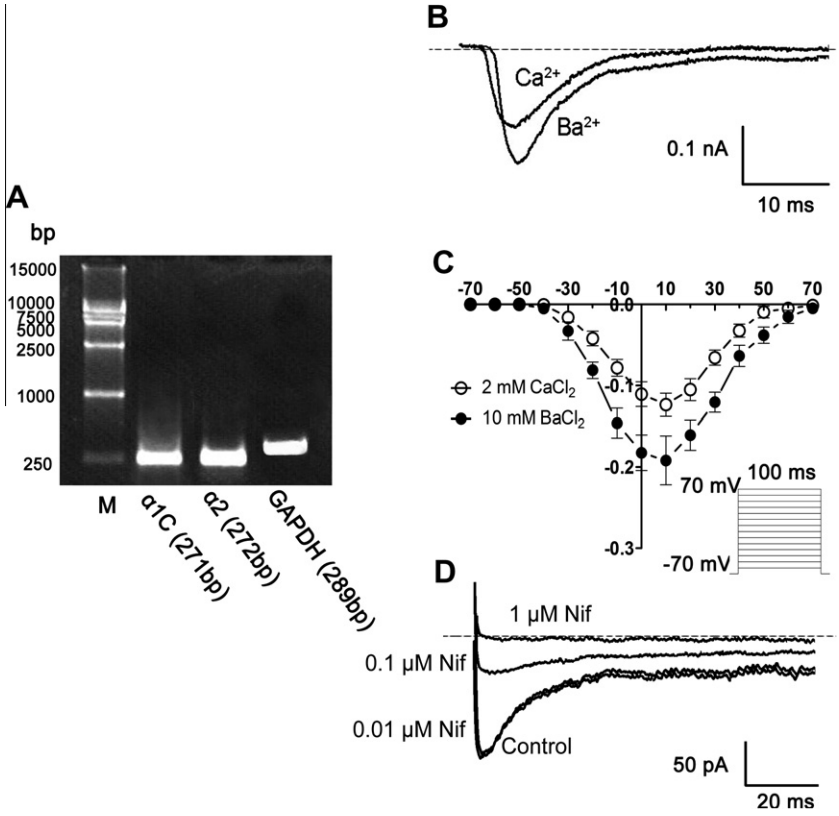

Fig. 2. (A) RT–PCR assay of the α1C and α2 subunits of $VDCC_L$ in rMSCs. M: DNA Marker DL15,000 (TaKaRa, Dalian, China). (B) Characteristics of I_{Ca} and I_{Ba} in rMSCs. Current traces were recorded by depolarizing steps from −70 mV to + 70 mV with 10 mV increments. (C) Corresponding current–voltage (I–V) relationships (n = 5). (D) Blockage of Ca^{2+} currents through $VDCC_L$ in rMSCs by Nif.

3.4. Effects of $VDCC_L$ on osteogenic differentiation of rMSCs

Alizarin Red S and ALP staining images showed that blockage of $VDCC_L$ decreased calcium nodule formation and ALP activity, respectively (Fig. 4A and B). The quantitative results of the calcium nodules, ALP positive regions, and OD values of ALP activities are shown in Fig. 4C–E. Compared to the control group, Nif inhibited mineralization by blocking the $VDCC_L$. After treating the cells with Nif, the relative mRNA expression of OCN, BSP, and Runx2 were reduced by 10–65% during osteogenic induction compared to the controls (Fig. 4H). Moreover, we transfected rMSCs with α1C-specific siRNA to down-regulate the α1C subunit, which is the functional subunit of $VDCC_L$. Knockdown induced a 60–85% reduction in α1C mRNA (Fig. 4F). Importantly, when α1C was reduced in these cells, the mRNA levels of OCN, BSP, and Runx2 were also reduced to 40–73% compared to control levels (Fig. 4G).

4. Discussion

MSCs are promising tools in the field of bone tissue regeneration because they can be easily isolated and expanded *in vitro*. However, it remains a challenge to promote the proliferation and differentiation of MSCs for bone tissue engineering. $VDCC_L$ mediates Ca^{2+} transport and intracellular Ca^{2+} signal transduction, which participate in diverse biological processes. They are usually expressed in several types of excitable cells, but also exist in non-excitable cells, such as osteoblasts and chondrocytes [15,16]. $VDCC_L$ are also expressed in rodent osteosarcoma [12] and rat osteoblast-like [17] cells. In recent years, some studies have shown that the mRNA of the $VDCC_L$ α1 subunit is expressed in undifferentiated hMSCs [18], and a functional $VDCC_L$ subunit is present in a small population (15%) of rat MSCs. In this study, we demonstrated by RT-PCR that the α1C and α2 subunits of $VDCC_L$ are highly expressed at the mRNA level in rMSCs, and we also detected the functional I_{Ca} of $VDCC_L$ in cultured rMSCs. The voltage-gated inward current was confirmed to be a Ca^{2+} channel current, because the current was elicited by depolarization from a holding potential of −70 mV and activated at −40 mV. Taking into account the fact that the inward current increased by approximately twofold upon substitution of Ca^{2+} with Ba^{2+} for the entire range of the potential recordings (Fig. 2C) and was completely blocked by Nif, we hypothesize that the I_{Ca} in rMSCs is mainly carried through $VDCC_L$.

$VDCC_L$ has been previously confirmed to be involved in the proliferation of MC3T3-E1 cells [19]. The α1C subunit of $VDCC_L$ plays a key role in bone growth *in vitro* [4]. In our studies, we first demonstrated that blocking $VDCC_L$ significantly inhibited rMSCs proliferation, as measured by growth curves and cell cycle analyses. Apoptosis, which is an important pathway of cell death, plays an essential role in tissue development and homeostasis [20,21]. Therefore, it is necessary to study factors that are involved in triggering MSC apoptosis in order to develop a new potential therapeutic measure that can effectively prevent cell loss after the establishment of tissue engineering models. Here, we found that $VDCC_L$ is a positive factor in protecting rMSCs from apoptosis, while the blockade of $VDCC_L$ leads to an increase in cell apoptosis.

It has been reported that blocking $VDCC_L$ in rats suppressed mechanically-induced bone formation [22]. However, an *in vitro* study showed that blocking $VDCC_L$ does not affect early osteogenic differentiation of human MSCs [23]. In contrast, Yoichi et al. demonstrated that $VDCC_L$ blockers (benidipine, amlodipine, and nifedipine) can increase ALP activity and stimulate mineral deposition

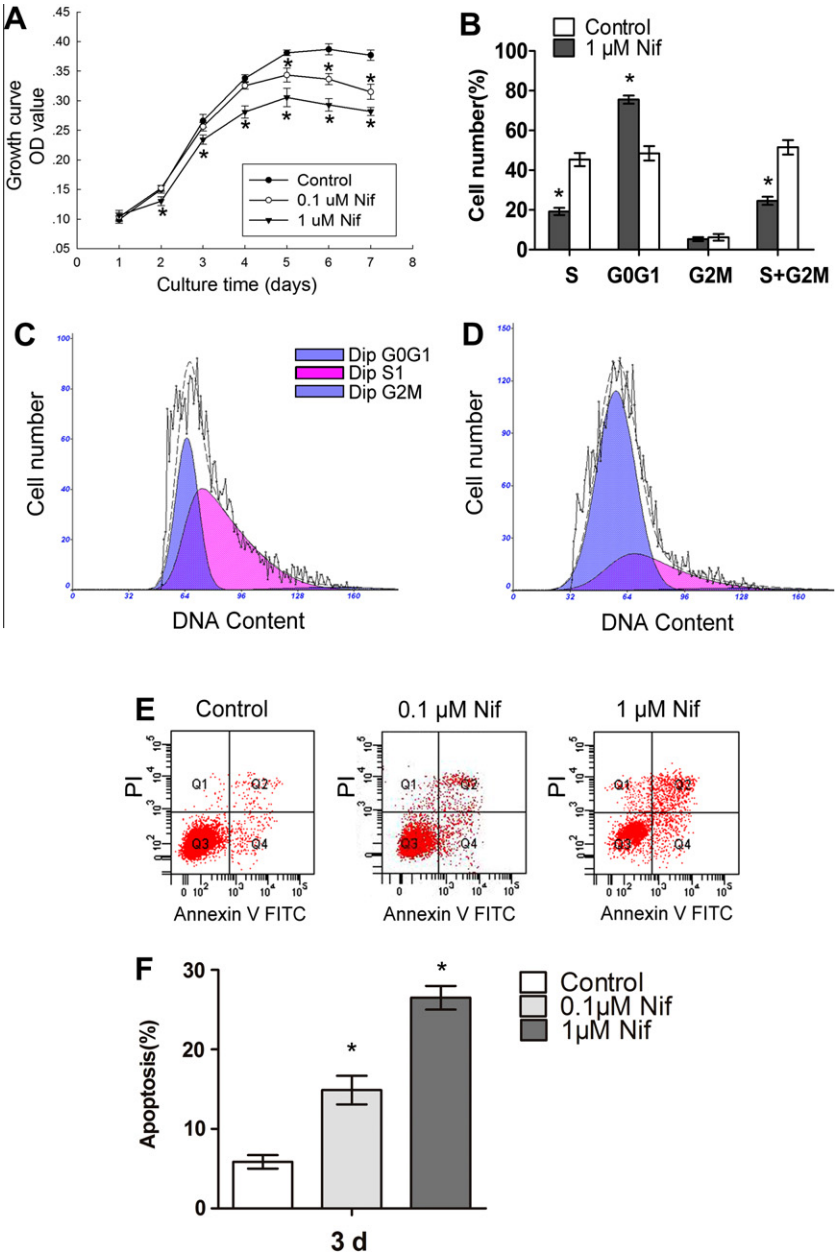

Fig. 3. (A) MTT assay results of rMSCs cultured in the control group and Nif-treated group ($n = 4$). (B) Flow cytometry analysis results of the cell cycle between two groups ($n = 7$). (C) Cell cycle of control group. (D) Cell cycle of 1 μM Nif-treated group. (E) Apoptosis results of rMSCs by flow cytometry. (F) Apoptotic rate analysis of different groups ($n = 4$). Data represent the mean ± standard deviation (SD). $^{*}P < 0.05$ vs. control group.

in mouse osteoblastic cells [24]. In the present study, we found that the $VDCC_L$ blocker Nif exerted dose-dependent inhibition on osteogenic differentiation of rMSCs. Several factors, such as species, cell types, procedures, and experiment conditions could explain these discrepancies. Most likely, the difference might be species and cell type related. Our study exhibited that incubation with 0.1 and 1 μM Nif resulted in a reduction in ALP activity and decreased density of ALP-positive cells compared to the untreated control group. ALP is a well-established osteoblast phenotypic marker [25], and the results presented here indicate that blockage of $VDCC_L$ affects osteogenic differentiation of rMSCs. Mineralized nodules, which occur in the final development of bone formation, were reduced in Nif-treated cells during osteogenic differentiation, confirming the function of $VDCC_L$ in the extracellular matrix mineralization of rMSCs *in vitro*. Moreover, real time PCR showed that blocking $VDCC_L$ markedly down-regulated the mRNA expression of OCN, BSP, and Runx2 during osteogenic differentiation of rMSCs. These proteins are considered to be osteoblast markers and play critical roles in contributing to bone formation. OCN, which is the most abundant noncollagenous protein in bone [26], is synthesized by osteoblasts and viewed as a marker for bone formation [27]. *In vitro* studies have shown that BSP is a marker of osteoblast differentiation and onset of mineral formation [28,29]. Runx2 is an important transcription factor required for osteoblast differentiation and bone formation [30]. Therefore, our data also provide genetic evidence for the positive role of $VDCC_L$ in the osteoblastic differentiation of rMSCs. However, Nif is not a specific blocker of $VDCC_L$. To exclude the non-specific pharmacological effects of Nif, we used RNAi-mediated α1C depletion to test the above findings. Previous studies have reported that α1C is the major functional subunit of $VDCC_L$, and mediates cell Ca^{2+} influx and the differentiation process [31]. Accordingly, α1C-specific siRNA was

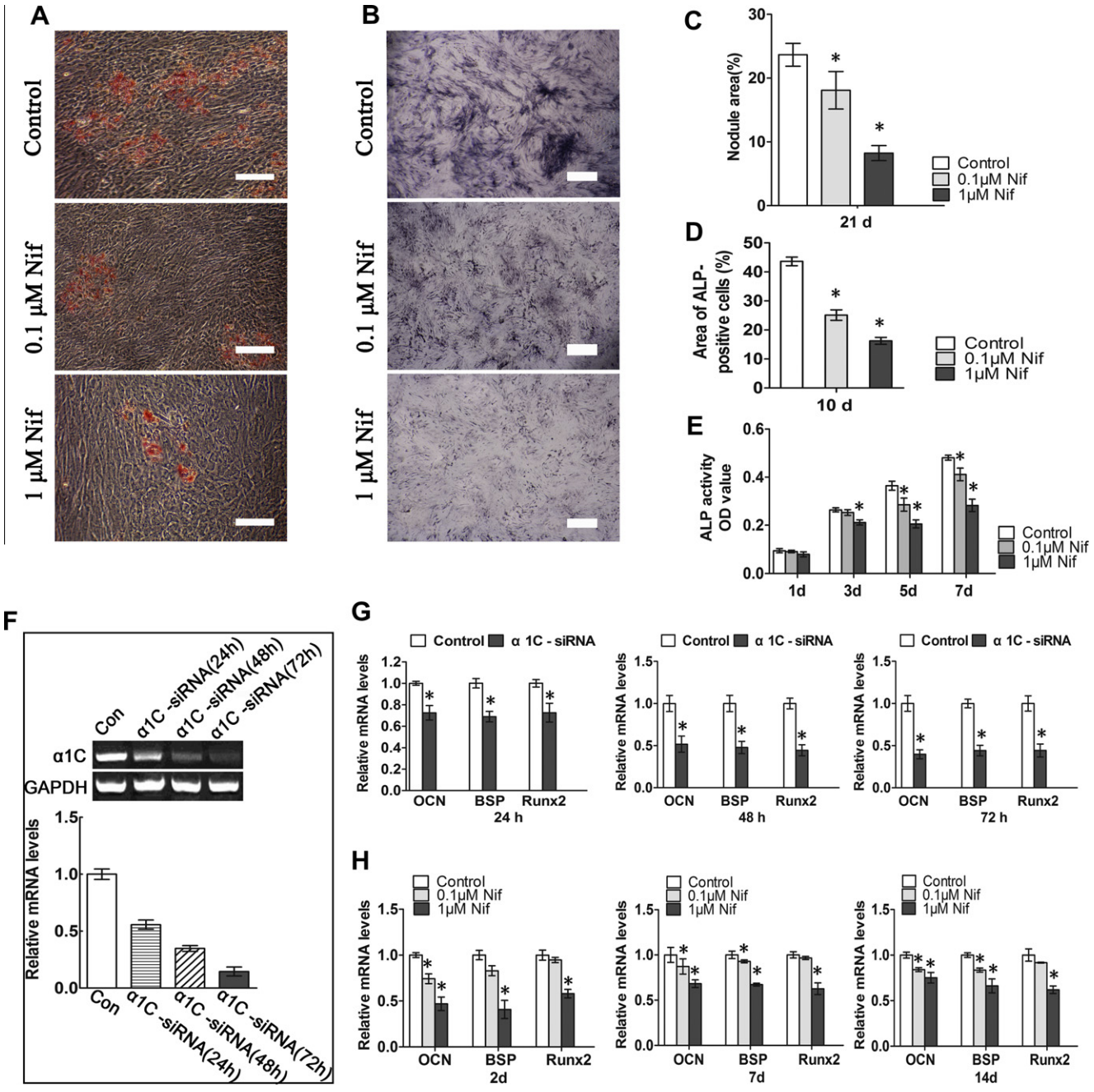

Fig. 4. (A) Images of Alizarin Red S stained rMSCs cultured in ODM with or without Nif (0.1 or 1 μM) for 21 d. (B) Images of ALP stained rMSCs cultured in ODM for 10 d. Bars = 50 μm. (C) Comparison of Alizarin Red S staining among different groups ($n = 10$). (D) Comparison of ALP staining among different groups ($n = 10$). (E) Comparison of ALP activity among different groups ($n = 7$). (F) Efficiency of α1C gene silencing. RT-PCR analysis of control and siRNA-transfected cells after 24, 48, and 72 h. Columns: relative expression level of α1C mRNA in control and siRNA-transfected groups ($n = 4$). (G) Real-time PCR results showed the mRNA level of OCN, BSP, and Runx2 in control and α1C siRNA group at 24, 48, and 72 h post-transfection ($n = 4$). (H) Real-time PCR assay after treatment of rMSCs with 0.1 and 1 μM Nif for 2, 7, and 14 days ($n = 4$). Data are presented as mean ± SD relative to control group (relative expression = 1.0) after normalization based on GAPDH. $^{*}P < 0.05$ vs. control group. (For interpretation of the references to colour in this figure legend, the reader is referred to the web version of this article.)

transfected into rMSCs to further test the effects of $VDCC_L$ on the cells and to examine whether the α1C subunit contributes to the regulating effects of $VDCC_L$. Similar to the effects of Nif treatment, α1C gene silencing also inhibited osteogenic differentiation of rMSCs. These observations suggest that the down-regulation of $VDCC_L$ suppresses osteogenic differentiation of rMSCs, and the α1C may be a primary functional subunit in $VDCC_L$-regulating processes. Meanwhile, we also investigated the effect of $VDCC_L$ on adipogenic differentiation of rMSCs, and the results showed non-significant difference in Nif treatment group and non-Nif treatment group (Supplementary Material). It suggests that adipogenic differentiation of rMSCs may not require $VDCC_L$ function.

In summary, the $VDCC_L$ are closely related to the functional activities of rMSCs. Inhibition of $VDCC_L$ down-regulates proliferation and osteogenic differentiation of rMSCs, but up-regulates apoptosis. Moreover, the α1C subunit may play an important role in the function of the channels. Our study has led to the intriguing notion that $VDCC_L$ may be novel regulatory factors for bone tissue

engineering. Further studies are needed to investigate the underlying mechanisms and use the potential function of Ca^{2+} channels as a target for regulating MSCs.

Acknowledgments

This study was supported by Wu Jieping Medical Foundation (Grant 320.6799.1140) and the National Nature Science Foundation of China (No. 81170982).

Appendix A. Supplementary data

Supplementary data associated with this article can be found, in the online version, at http://dx.doi.org/10.1016/j.bbrc.2012.06.128.

References

[1] A. Croft, S. Przyborski, Mesenchymal stem cells from the bone marrow stroma: basic biology and potential for cell therapy, Curr. Anaesth. Crit. Care 15 (2004) 410–417.
[2] U. Lakshmipathy, C. Verfaillie, Stem cell plasticity, Blood Rev. 19 (2005) 29–38.
[3] D. Hanley, J. Brown, A. Tenenhouse, W. Olszynski, G. Ioannidis, C. Berger, J. Prior, L. Pickard, T. Murray, T. Anastassiades, Associations among disease conditions, bone mineral density, and prevalent vertebral deformities in men and women 50 years of age and older: cross-sectional results from the canadian multicentre osteoporosis study, J. Bone Miner. Res. 18 (2003) 784–790.
[4] Y. Shao, M. Alicknavitch, M.C. Farach-Carson, Expression of voltage sensitive calcium channel (VSCC) L-type Cav1. 2(α1C) and T-type Cav3. 2 (α1H) subunits during mouse bone development, Dev. Dyn. 234 (2005) 54–62.
[5] D. Triggle, Calcium, calcium channels, and calcium channel antagonists, Can. J. Physiol. Pharmacol. 68 (1990) 1474.
[6] D. Chesnoy-Marchais, J. Fritsch, Voltage-gated sodium and calcium currents in rat osteoblasts, J. Physiol. 398 (1988) 291.
[7] B. Ye, Ca^{2+} oscillations and its transporters in mesenchymal stem cells, Physiol. Res. 59 (2010) 323–329.
[8] E. Barry, F. Gesek, A. Yu, J. Lytton, P. Friedman, Distinct calcium channel isoforms mediate parathyroid hormone and chlorothiazide-stimulated calcium entry in transporting epithelial cells, J. Membr. Biol. 161 (1998) 55–64.
[9] G.R. Li, X.L. Deng, H. Sun, S.S. Chung, H.F. Tse, C.P. Lau, Ion channels in mesenchymal stem cells from rat bone marrow, Stem Cells 24 (2006) 1519–1528.
[10] W.A. Catterall, Structure and regulation of voltage-gated Ca^{2+} channels, Annu. Rev. Cell Dev. Biol. 16 (2000) 521–555.
[11] I. Serysheva, S. Ludtke, M. Baker, W. Chiu, S. Hamilton, Structure of the voltage-gated L-type Ca^{2+} channel by electron cryomicroscopy, Proc. Nat. Acad. Sci. USA 99 (2002) 10370.
[12] J.J. Bergh, Y. Shao, K. Akanbi, M.C. Farach-Carson, Rodent osteoblastic cells express voltage-sensitive calcium channels lacking a gamma subunit, Calcif. Tissue Int. 73 (2003) 502–510.
[13] O.P. Hamill, A. Marty, E. Neher, B. Sakmann, F. Sigworth, Improved patch-clamp techniques for high-resolution current recording from cells and cell-free membrane patches, Pflügers Arch. Eur. J. Physiol. 391 (1981) 85–100.
[14] K.J. Livak, T.D. Schmittgen, Analysis of relative gene expression data using real-time quantitative PCR and the 2-[Delta][Delta] CT method, Methods 25 (2001) 402–408.
[15] M.J. Zuscik, T.E. Gunter, J.E. Puzas, R.N. Rosier, Characterization of voltage-sensitive calcium channels in growth plate chondrocytes, Biochem. Biophys. Res. Commun. 234 (1997) 432.
[16] X.T. Wang, S. Nagaba, Y. Nagaba, S.W. Leung, J. Wang, W. Qiu, P.L. Zhao, S.E. Guggino, Cardiac L-type calcium channel α1C subunit is increased by cyclic adenosine monophosphate: messenger RNA and protein expression in intact bone, J. Bone Miner. Res. 15 (2000) 1275–1285.
[17] P. Morain, J.L. Peglion, E. Giesen-Crouse, Ca^{2+} channel inhibition in a rat osteoblast-like cell line, UMR 106, by a new dihydropyridine derivative, S11568, Eur. J. Pharmacol. 220 (1992) 11–17.
[18] E.M. Graf, M. Bock, J.F. Heubach, I. Zahanich, S. Boxberger, W. Richter, J.H. Schultz, U. Ravens, Tissue distribution of a human Cav1. 2 [alpha] 1 subunit splice variant with a 75 bp insertion, Cell Calcium 38 (2005) 11–21.
[19] J.J. Bergh, Y. Xu, M.C. Farach-Carson, Osteoprotegerin expression and secretion are regulated by calcium influx through the L-type voltage-sensitive calcium channel, Endocrinology 145 (2004) 426.
[20] X.F. Xu, B.L. Cai, S.M. Guan, Y. Li, J.Z. Wu, Y. Wang, B. Liu, Baicalin induces human mucoepidermoid carcinoma Mc3 cells apoptosis in vitro and in vivo, Invest. New Drugs 29 (2011) 637–645.
[21] A.P. Arrigo, In search of the molecular mechanism by which small stress proteins counteract apoptosis during cellular differentiation, J. Cell. Biochem. 94 (2005) 241–246.
[22] J. Li, R.L. Duncan, D.B. Burr, C.H. Turner, L-type calcium channels mediate mechanically induced bone formation in vivo, J. Bone Miner. Res. 17 (2002) 1795–1800.
[23] I. Zahanich, E.M. Graf, J.F. Heubach, U. Hempel, S. Boxberger, U. Ravens, Molecular and functional expression of voltage-operated calcium channels during osteogenic differentiation of human mesenchymal stem cells, J. Bone Miner. Res. 20 (2005) 1637–1646.
[24] Y. Nishiya, S. Sugimoto, Effects of various antihypertensive drugs on the function of osteoblast, Biol. Pharm. Bull. 24 (2001) 628–633.
[25] P. Ducy, R. Zhang, V. Geoffroy, A.L. Ridall, G. Karsenty, Osf2/Cbfa1: a transcriptional activator of osteoblast differentiation, Cell 89 (1997) 747–754.
[26] Q.Q. Hoang, F. Sicheri, A.J. Howard, D.S.C. Yang, Bone recognition mechanism of porcine osteocalcin from crystal structure, Nature 425 (2003) 977–980.
[27] P. Hauschka, Osteocalcin: the Vitamin K-dependent Ca< sup> 2+</sup>-binding protein of bone matrix, Pathophysiol. Haemost. Thromb. 16 (1986) 258–272.
[28] J.A.R. Gordon, C.E. Tye, A.V. Sampaio, T.M. Underhill, G.K. Hunter, H.A. Goldberg, Bone sialoprotein expression enhances osteoblast differentiation and matrix mineralization in vitro, Bone 41 (2007) 462–473.
[29] O. Frank, M. Heim, M. Jakob, A. Barbero, D. Schäfer, I. Bendik, W. Dick, M. Heberer, I. Martin, Real-time quantitative RT-PCR analysis of human bone marrow stromal cells during osteogenic differentiation in vitro, J. Cell. Biochem. 85 (2002) 737–746.
[30] R.T. Franceschi, G. Xiao, Regulation of the osteoblast-specific transcription factor, Runx2: responsiveness to multiple signal transduction pathways, J. Cell. Biochem. 88 (2003) 446–454.
[31] Y. Nishiya, N. Kosaka, M. Uchii, S. Sugimoto, A potent 1,4-dihydropyridine L-type calcium channel blocker, benidipine, promotes osteoblast differentiation, Calcif. Tissue Int. 70 (2002) 30–39.